Global and Local Expression of Chirality in Serine on the Cu{110} Surface

Article

Global and Local Expression of Chirality in Serine on the Cu{110} Surface

Tugce Eralp,[†] Andrey Shavorskiy,[†] Zhasmina V. Zheleva,[†] Georg Held,[*,†] Nataliya Kalashnyk,[‡] Yanxiao Ning,[‡] and Trolle R. Linderoth[‡]

University of Reading, Department of Chemistry, Whiteknights, Reading, UK, and

Interdisciplinary Nanoscience Center (iNANO) and Department of Physics and Astronomy,

Aarhus University, Denmark

E-mail: g.held@reading.ac.uk

TOC Graphics
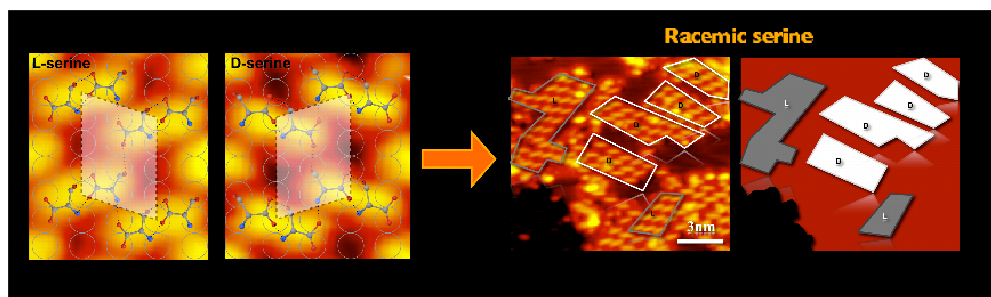
[†]University of Reading

[‡]Aarhus University

Abstract

Establishing a molecular-level understanding of enantioselectivity and chiral resolution at organic-inorganic interfaces is a key challenge in the field of heterogeneous catalysis. As a model system we investigate the adsorption geometry of serine on Cu{110} using a combination of low-energy electron diffraction (LEED), scanning tunneling microscopy (STM), X-ray photoelectron spectroscopy (XPS), and near edge X-ray absorption fine structure (NEXAFS) spectroscopy. The chirality of enantiopure chemisorbed layers, where serine is in its deprotonated (anionic) state, is expressed at three levels: (i) the molecules form dimers whose orientation with respect to the substrate depends on the molecular chirality, (ii) dimers of L and D enantiomers aggregate into superstructures with chiral $(-1 \mp 2; 4\ 0)$ lattices, respectively, that are mirror images of each other, and (iii) small islands have elongated shapes with the dominant direction depending on the chirality of the molecules. Dimer and superlattice formation can be explained in terms of intra and inter-dimer bonds involving carboxylate, amino and $\beta-$OH groups. The stability of the layers increases with the size of ordered islands. In racemic mixtures we observe chiral resolution into small ordered enantiopure islands, which appears to be driven by the formation of homochiral dimer subunits and the directionality of inter-dimer hydrogen bonds. These islands show the same enantiospecific elongated shapes as in low-coverage enantiopure layers.

Introduction

Amino acids are the main building blocks of advanced biomolecules such as peptides and proteins but also as single molecules they play an important role as chiral modifiers in biomineralization and catalysis (see e.g. [1–7] and references therein). All natural amino acids except glycine have a chiral center and can, thus, introduce chirality to achiral inorganic surfaces. Such chiral modification is expressed either through a direct enantioselective interaction between adsorbed molecules in the sense of molecular recognition or through a global modification of the entire surface by forming chiral molecular superstructures or inducing chiral surface reconstructions. Such effects are used to template heterogenous transition metal catalysts such that one product enantiomer is preferred over the other or by stereodirecting the reactants in the transition state. [4,8,9]

In order to gain a more fundamental understanding of these templating effects, amino acid adsorption was studied on a number of metal single crystal surfaces including gold, platinum, palladium, nickel and copper. [10–40] The largest data base exists for adsorption on Cu surfaces, partly because on these amino acids tend to form ordered superstructures and adsorb in well-defined adsorption geometries, which makes them good model systems to be studied with a variety of surface science techniques, such as scanning tunneling microscopy (STM), low-energy electron diffraction (LEED), X-ray photoelectron spectroscopy (XPS), near edge X-ray absorption fine structure spectroscopy (NEXAFS), reflection absorption infrared spectroscopy (RAIRS) and photoelectron diffraction (PhD). On Cu{110} small amino acids, such as glycine, alanine, proline and norvaline, usually adsorb in their anionic form at room temperature with a deprotonated carboxylic acid and an intact amino group ($RCHNH_2COO$). [3,10,12,13,17,21,22,24–26,31,34,39] The amino group nitrogen atom and the two oxygen atoms of the COO group form bonds with one Cu atom each leading to an asymmetric triangular footprint on the surface. In addition to the common $p(3 \times 2)$ or $p(4 \times 2)$ superstructures, chiral amino acids can also form structures expressing global (lattice) chirality, where the lattices formed by opposite enantiomers are non-superimposable mirror images of each other. [3,21] In all superstructures intermolecular interactions, either hydrogen bonds or repulsive interactions between the side chain groups, play an important role and can lead to significant dif-

ferences in the adsorption properties, such as changes in the molecular orientation or dimerization on the surface.[24–26,31,39]

Serine has an OH group at the β-position in addition to the amino acid functional groups, NH_2 and COOH; models of L and D-serine are shown in Figure 1. Although magic number gas-phase clusters of serine have been investigated widely,[41,42] there are not many examples of serine adsorption on metal surfaces. In a recent review Barlow and Raval reported an ordered LEED pattern for the high coverage of L-serine on Cu{110} when annealed to 400 K.[3] They suggested that intermolecular H-bonding involving the β-OH groups affects the ordering of the molecules on the surface. In an STM study of L-serine adsorbed on Cu{100} Iwai et al. observed "peanut-shaped" dimers.[29] The authors assumed the usual bonding to the substrate, through the nitrogen atom and the COO oxygens, and suggested that the dimers involve hydrogen bonds between the NH_2 and the COO groups of molecules with opposite orientation. Their model involves two additional H-bonds between carboxylate oxygens and β-OH and NH_2 groups, respectively, linking the dimers to each other.

In the present article, we study in detail the adsorption properties and intermolecular interactions of L, D and racemic serine on Cu{110} using LEED, STM, XPS, NEXAFS and temperature-programmed desorption (TPD). We observe the formation of enantiopure dimers for all adsorbate compositions, even for racemic mixtures. From NEXAFS the orientation of the carboxylate group could be determined, which indicates that dimerization on the Cu{110} substrate occurs through a type of H-bonding interaction, which is different from the one observed for Cu{100}. As a consequence, long-range ordered islands with globally chiral superstructures are formed, which have the same periodicity for all coverages. Racemic layers are separated into enantiopure islands with the corresponding superstructures.

Experiment

The experiments were carried out in three different ultrahigh vacuum (UHV) chambers. The first chamber at Reading University is dedicated to LEED and TPD experiments; a second chamber at iNANO, Aarhus University, was used for the STM experiments; the third UHV chamber is the endstation of the bending magnet beam line BEAR at the Elettra Synchrotron Radiation Facility in Trieste, Italy, which was used for XPS and angle-resolved NEXAFS experiments. In all UHV systems the base pressure was in the low 10^{-10} mbar range. The Cu samples were cleaned using standard procedures including electro-polishing, Ar^+ ion sputtering and a final annealing step to 1000 K in UHV.[43] L, D and racemic serine was purchased from Sigma-Aldrich (99% purity) and vapor deposited onto the sample at room temperature. The molecules were evaporated from a glass crucible inside a stainless steel tube, which was resistively heated to ensure homogeneous temperature distribution across the crucible. **The evaporant was degassed at** $120°$**C for about 2 hours before deposition; during deposition the temperature was kept at** $150°$**C, which led to a pressure rise to about** 4×10^{-9} **mbar in the UHV chamber.**

For both XPS and NEXAFS experiments at Elettra, a purpose-built 66 mm spherical deflector electron analyzer was used to detect Auger and photoelectrons. The photon energies used for the C 1s, N 1s and O 1s XP spectra were 400 eV, 510 eV, and 635 eV, respectively, with a combined energy resolution (monochromator and analyzer) of approximately 0.5 eV. The binding energies (BE) were calibrated with respect to the Fermi edge using the same photon and pass energies as for the measurements. For O-NEXAFS the signal of oxygen KLL Auger electrons was recorded in the kinetic energy range 499-517 eV. **All NEXAFS experiments were performed with linearly polarized synchrotron radiation at normal incidence but the in-plane angle of the polarization vector was varied by rotating the sample together with the analyzer over a range of** $135°$ **from the** $[\bar{1}10]$ **direction (parallel to the close packed rows of Cu atoms). The sample orientation was determined by LEED. The photon energy scale was calibrated by an offset such that the position of the** π^***-resonance coincides with that in NEXAFS spectra previously published for alanine and glycine on Cu{110}.[31,44]** Before each experiment the cleanliness of the sample was

checked with XPS and surface contamination was always found to be less than 0.01 ML (1 ML = 1 adsorbate atom/molecule per substrate unit cell). In order to define the relative serine coverage, XP spectra (C 1s, N 1s, O 1s) were recorded while stepwise increasing the coverage until the multilayer signal was observed. The sample temperature was measured with a pyrometer.

For the experiments at Reading a low current multi-channelplate LEED instrument was used to record the diffraction patterns for electron energies ranging from 25 eV to 250 eV. No significant beam damage was seen for up to 30 min observation time if the beam current was below 100 nA. The bright ring observed for energies above 50 eV is an artifact of the imaging mode of the low-current LEED system. Each LEED experiment was followed by TPD experiments (constant heating rate of 3K/s) measuring the partial pressures of the decomposition products H_2 (mass 2) and CO_2 (mass 44) with a quadrupole mass spectrometer in order to calibrate the coverage. **The mass spectrometer was housed in a differentially pumped gold-plated Cu tube, similarly to the "Feulner-Cup" design[45] with an aperture of 5 mm diameter, which is roughly half the size of the sample. The sample was kept at a distance of 1 mm from the aperture during the TPD experiments in order to maximize the desorption signal from the surface. The mass spectrometer was also used to check the purity of serine during deposition.** The temperature was measured through a thermocouple attached to the molybdenum sample plate.

The STM experiments were performed using a home-built Aarhus-type STM.[46] **The imaging parameters were optimized for each set of images to provide the best possible resolution and slightly different parameters were therefore used in the images reported. Within the band of values used for the results presented here, we did not observe any systematic variations in the imaging of the serine molecules on Cu{110}.** All dosing and annealing was done *in situ* with the sample transferred to the main manipulator. Temperatures were measured with a thermocouple pressed against the back of the sample and connected through terminals on the main manipulator. A slightly different evaporator design was used in the Aarhus experiments with the glass crucibles heated by a coil of thin wire. Due to the different methods of temperature reading at the three different experimental stations different temperatures were measured for the ordering of the serine

layers. In the STM experiments, the ordered phase was found at a temperature reading of 370 K, whereas in the LEED experiments ordering was only obtained at 420 K. We consider the latter temperature reading more accurate.

Results

LEED and TPD

In order to determine the long-range periodicity and to characterize the general temperature and coverage-dependent adsorption behavior of serine on Cu{110}, LEED and TPD experiments were performed for different overlayers of L, D and racemic serine. **The experiments were performed for two different coverages deposited at room temperature on Cu{110}, low coverage around 0.1 ML (deposition time 10 min) and saturation coverage of 0.25 ML (deposition time 60 min).** The absolute saturation coverage was determined from the size of the unit cell observed in LEED assuming that it contains two molecules (for justification see STM results below). Lower coverages were calibrated relative to saturation, by comparing the areas under the TPD spectra for the decomposition products H_2 (mass 2) and CO_2 (mass 44), as shown in Figure 4 (all spectra were recorded after obtaining the related LEED patterns discussed below). The molecular mass of serine could not be detected in the mass spectrum.

For both coverages, 0.1 ML and 0.25 ML, of L-serine and D-serine the same type of LEED pattern of ordered superstructures was observed, $(-1\ -2;\ 4\ 0)$ and $(-1\ +2;\ 4\ 0)$, respectively (see Figure 2), in agreement with Ref.[3] The two superstructure lattices comprise 8 Cu atoms each and do not share any symmetry with the Cu{110} surface other than a rotation by $180°$. They are mirror images of each other, therefore the surface chirality is expressed on a global scale, not just on the molecular level, unlike the more common achiral $p(3 \times 2)$ superstructure, which has been observed for a number of other small amino acids on Cu{110}, such as glycine, norvaline, and alanine.[3,12,13,21,22]

For the low coverage layers the superstructure was observed already at room temperature with-

out annealing. In the corresponding LEED patterns the spots are uniaxially broadened, indicating small elongated islands of the molecules. The directions of spot broadening in reciprocal space are perpendicular to the directions of island growth (i.e. the direction of island elongation) in real space. The latter are indicated by the vectors $\vec{w}_1$ and $\vec{w}_2$ in the middle panel of Figure 2 for the two enantiomers. For saturation coverage no LEED pattern was observed at room temperature, however after annealing to 420 K the same ordered LEED pattern is obtained as for low coverages $((-1\ -2;\ 4\ 0)$ for L-serine and $(-1\ +2;\ 4\ 0)$ for D-serine, see bottom panel of Figure 2). Annealing is necessary because of a lack of mobility at room temperature trapping the chemisorbed molecules in a disordered phase, which possibly also involves adsorption on top of the first layer (see also STM, XPS and NEXAFS results below). After annealing the saturated chemisorbed layer superstructure has sharper and more intense spots than for 0.1 ML.

The LEED pattern for the racemic mixture of serine shows superstructures for coverages between 0.10 and 0.25 ML which are superpositions of the LEED patterns of the two enantiomers, see Figure 3. The strongest LEED spots are those where the spots of the two enantiomer structures overlap. This indicates that the racemic layer consists of enantiopure domains each giving rise to the LEED pattern of either the L or D-enantiomer.

The TPD spectra and desorption temperatures are very similar for enantiopure L and D-serine, see Figure 4. The simultaneous desorption of H_2 and CO_2 marks the dissociation of serine on the surface, which is initiated by the cleavage of the backbone C-C bond at the respective temperatures.[21] XPS shows intact molecules up to the first desorption peak (see below) and C and N-containing dissociation products above 560 K (not shown). The specific assignment of the two features seen in each of the spectra is difficult as there are no structural data available for these temperatures. A likely scenario is that the sharper low-temperature feature is connected with the breaking up of close-packed hydrogen-bonded islands and a rearrangement into a less densely packed configuration, possibly stabilized by dissociation products left on the surface; the second feature marks the dissociation of these molecules. For 0.11 ML and 0.07 ML coverages of L and D-serine, respectively, a first desorption

peak appears at 442 K followed by a second peak at 523 K. The saturated chemisorbed layer (0.25 ML annealed to 420 K), shows desorption peaks at 470 K and 520 K. The shift of the first peak by 28 K towards higher temperatures indicates additional stabilization at the higher coverage and, hence, a net attractive interaction between the serine molecules. The desorption peaks of the racemic layer appear at significantly lower temperatures than for the enantiopure layers, especially at saturation (438 K and 515 K for 0.1ML and 454 K and 515 K for 0.25 ML), which is a further indication for the formation of small islands. **The areas under the spectra for the saturation coverages are the same, within $\pm 5\%$, for the enantiopure layers and about 25% higher for the racemic layer. The latter difference may be a combination of different packing densities and slightly different dissociation probabilities in the racemic and enantiopure layers.**

STM

The molecular assembly and island growth behavior in real space was studied by STM for enantiopure and racemic layers of serine on Cu{110}. Figure 5(a-c) shows STM images of adsorption structures of D-serine with increasing coverage obtained after deposition at room temperature (300 K). At low coverage, well-ordered molecular islands decorate step edges with growth primarily occurring on the upper terraces (Figure 5(a)). When the coverage approaches saturation of the first layer, the D-serine molecules form less ordered islands (Figure 5(b) and (c)) with additional bright features indicating adsorption of molecules on top of the chemisorbed layer. A close-up view of such an island is displayed in Figure 6(Ia). Two types of features are readily identified within the island in the form of elongated and near-circular protrusions. Height profiles across these features are displayed in Figure 6(Ib); they show that the near-circular protrusions are approximately 5 Å in diameter (pink curve) while the length of the elongated protrusions is 10 Å (green curve). The extension of the elongated features is too large to match the size of individual serine molecules and the presence of large numbers of smaller protrusions also suggests that the larger ones consist of molecular agglomerates. We therefore attribute them to serine dimers and the near-circular protrusions to serine monomers. The individual serine molecules in the dimer

features are barely distinguishable, as evidenced from the almost flat height profile of the dimer protrusions. In some cases, elongated features with a distinct central minimum are observed (purple curves), which are attributed to two monomers in close proximity. For the as-deposited layer closer to saturation coverage, the disordered islands are primarily composed of monomers mixed with some dimers (Figure 5(c) and Figure 6(Ia)). If these structures are annealed at 350-370 K, however, all monomers merge into dimers and the ordering improves significantly leading to regular molecular patterns, as shown in Figure 5(d).

The aggregation behavior is observed to be similar for enantiopure D- and L-serine. A distinct signature of the molecular chirality is seen in the well-ordered islands formed from serine dimers. This is illustrated in Figure 6(IIa) and (IIb) showing islands grown from L-serine and D-serine, respectively. In addition to forming mirrored superstructure lattices, the long axes of the L-/D-serine dimers are rotated by $\mp 73°$, respectively, from the indicated $[\bar{1}10]$ direction of the substrate. The intrinsic chirality of the serine molecules is thus expressed in the adsorption orientation of the serine dimers and, by regular stacking of the dimers, extends to a global chirality of the entire molecular layers. As mentioned before, the superstructures are mirror images of each other, related by reflection in a plane along the $[\bar{1}10]$ direction. (Note that this mirror-image relation is emphasized in Figure 6(IIa,b) by showing cut-outs of STM images, rotated to make the $[\bar{1}10]$ direction vertical.)

Unit cells for the regular dimer overlayers are shown in Figure 6(IIa,b). The lengths of the unit cell vectors, as derived from the STM images, are $|\vec{b}_1| = 7.7$ Å and $|\vec{b}_2| = 9.9$ Å with an angle of $110°$ between them and $\vec{b}_2$ parallel to the substrate $[\bar{1}10]$ direction. These observations are entirely consistent with the $(-1 \mp 2; 4\ 0)$ superlattice unit cells derived from the LEED experiments, which lead to values of $|\vec{b}_1| = 7.65$ Å and $|\vec{b}_2| = 10.20$ Å and an angle of $109.5°$. Also, the observed disappearance of the LEED pattern with increasing coverage and re-emergence upon annealing is consistent with the growth behavior illustrated in the sequence of STM images of Figure 5: ordered small islands (a) $\rightarrow$ disorder (b,c) $\rightarrow$ ordered large islands (d). The observed LEED pattern for low coverage showed streaky spots suggesting domain broadening along the direction of the short

unit cell diagonal. The STM data provide a real-space explanation for this observation in terms of a preferred island growth direction. Figure 6(IIa,b) show rows of tilted serine dimers along the short unit cell diagonal, which define the prevalent regular island edges. Larger scale STM images in Figure 6(III), which were recorded for intermediate coverage, show that this leads to a preferred island growth along this direction, indicated by the vectors $\vec{w}_1$ and $\vec{w}_2$ for L- and D-serine, respectively. This suggests that the interaction between the dimers is stronger in the direction of w_1/w_2 compared to the other inter-row direction along b_1.

In Figure 7 we show two representative STM images of a racemic layer at an intermediate coverage of 0.17 ML obtained using the same experimental conditions as for the enantiopure layers, including annealing to 370 K. The structure consists of comparatively small locally ordered domains formed from elongated features identical to those attributed to enantiopure serine dimers above. No additional features have been found. While the STM signature of a heterochiral (racemic) LD-serine dimer is not known, the data strongly suggest that intermolecular chiral recognition favors the formation of homochiral (enantiopure) serine dimers. We therefore assign the elongated features to L and D serine dimers, respectively, based on their rotation with respect to the underlying Cu{110} surface lattice. Approximately equal numbers of L- and D-like dimers are found predominantly arranged in islands with the same local periodicities and the same anisotropic shapes as the corresponding enantiopure islands.

Photoelectron (XPS) and Photoabsorption (NEXAFS) Spectroscopy

In order to gain more detailed information about the nature of the local adsorption geometry and the chemical state of the functional groups within the molecular structure, photoemission (XPS) and photoabsorption (NEXAFS) experiments were carried out. XPS spectra were recorded in the C 1s, N 1s and O 1s regions for D-serine on Cu{110} for different coverages and heat treatments, see Figure 8. The N 1s spectra (Figure 8(a)) clearly indicate that the amino group is in a neutral NH_2 state for serine molecules in the chemisorbed layer. The single peak with binding energy (BE) between 399.4 eV (0.10 ML) and 399.9 eV (0.25 ML) is typical for amino (NH_2) groups, which

are involved in a bond with Cu surface atoms.[31,37,44] The changes in binding energy and peak width between the two coverages and upon annealing are related to different degrees of hydrogen bonding in these layers. The additional high BE peak at 402.2 eV in the spectrum for the serine multilayer is typical for NH_3^+ and would be expected for zwitterionic amino acids, which are more stable in the condensate phase.[31,47,48]

The O 1s spectra (Figure 8(b)) for the chemisorbed layers always show two peaks around 531.5 eV and 533.0 eV. The low BE peak has also been observed for alanine and glycine on Cu surfaces and is attributed to de-protonated oxygen atoms of the carboxylic acid group (COO), which are involved in a bond with the surface.[31,37,44] The high BE peak is typical for "dangling" OH groups and can be associated with neutral carboxylic acid groups (COOH) and/or the OH group at the β position. A O 1s peak at BE 533.1 eV was previously observed for non-bonded hydroxyl groups of L-DOPA and tyrosine-terminated propanethiol on Au substrates.[49,50] The ratios between the low and high BE peak areas are 2.5 : 1 for 0.10 ML, 1 : 1 for 0.25 ML at room temperature, and 1.5 : 1 for 0.25 ML after annealing to 420 K. Considering that photoelectron diffraction can cause significant deviations from stoichiometric peak ratios, this is consistent with the triangular bonding pattern involving bonds through the two oxygen atoms of a deprotonated carboxylic group and the amino group, which has been found for a number of small amino acids on Cu surfaces.[3,31,37,40] For serine the expected peak ratio would be 2 : 1 (two oxygen atoms in the deprotonated carboxylate group vs β-OH). The smaller relative area of the low BE peak in the spectrum of the un-annealed layer at 0.25 ML indicates that not all carboxylate groups are de-protonated, which is most likely the reason for the observed lack of order in this layer. The multilayer O 1s spectrum is consistent with the zwitterionic form of serine, for which one would also expect a peak ratio of 2 : 1. The overall shift to higher BE observed in all multilayer spectra is due to the lack of metal screening.

Three peaks are resolved in the C 1s spectrum for 0.1 ML serine (Figure 8(c)). By comparison with similar adsorption systems we assign the peak at 288.0 eV to the carboxylate carbon atom, the peak at 286.1 eV to the α-carbon, and the peak at 284.7 eV the β-carbon atom.[23,31,37,47,51] With increasing coverage, all three peaks shift to higher BE, whereby the β-carbon signal is affected the

12

most, shifting by 0.9 eV. This corresponds to an energy shift of 0.4 eV in the N 1s peak. There is little change in the spectrum when the saturated layer is annealed to 420 K because none of the carbon atoms is directly involved in a surface bond. In the multilayer spectrum, however, both α and β-carbon peaks show large relative shifts, caused by the change into the zwitterionic state, which affects the charge distribution at both carbon atoms.

The azimuthal orientation of the serine molecules can be determined from the angular dependence of the oxygen K-edge NEXAFS spectra. The sharp resonance at 533.1 eV (see Figure 9) is caused by the excitation of O 1s electrons into the unoccupied π^* orbital located at the carboxylate group (O-C-O). According to dipole selection rules, the intensity of this peak is at a maximum when the polarization vector of the exciting synchrotron radiation is perpendicular to the O-C-O triangle and goes to zero when it lies in the plane of the triangle.[52] The π^*-resonance is followed by two broad σ resonance peaks, which are associated with C-C, C-O and C-N σ-bonds.[31,44]

Figure 9 shows a selection of O NEXAFS spectra for 0.1 ML and 0.25 ML D-serine adsorbed at 300 K and 0.25 ML annealed to 420 K. Spectra were taken at normal incidence with different in-plane orientations of the polarization vector between $0°$ (parallel to the $[\bar{1}10]$ direction of the close packed rows of Cu atoms) and $135°$. For clarity only the $0°$ and $-90°$ spectra are shown in Figure 9(a). The π^*-resonance shows strong polarization dependence for 0.10 ML and 0.25 ML after annealing. These are the same layers for which ordered molecular structures were observed in LEED and STM. The spectra of the un-annealed saturated layer, however, do not show significant polarization dependence in accordance with the lack of order found in LEED and STM. For the ordered layers the maximum intensity of the π^*-resonance is observed when the polarization vector is perpendicular to the close packed rows ($-90°$), which indicates that the carboxylate groups are oriented nearly parallel to these rows. The annealed saturated layer shows an additional peak at 536 eV for $-90°$, which was associated earlier by Nyberg et al. with H-bonding interaction between NH_2 and COO oxygen.[20] We get more precise information about the molecular orientation from fitting the normalized and background-subtracted peak heights of the π^* resonance for different angles with the expected angular dependence assuming that the two molecules in the serine

dimer have different orientations:

$$I_\pi(\phi) = I_{max} \cdot (cos^2(\phi - \alpha_1) + cos^2(\phi - \alpha_2))$$

Here, ϕ is the in-plane angle of the polarization vector and α_1/α_2 are angles describing the azimuthal orientation of the carboxylate groups of the two serine molecules (see Figure 10(a) for definition; for a more detailed description of the data analysis see[31,37,40]). **The latter two angles and I_{max} are the only free fit parameters, therefore four data points are sufficient to extract these values. The data and best fit function for the annealed 0.25 ML D-serine layer are shown in Figure 9(b). The best fit is achieved for angles of $\alpha_1 = (-79 \pm 3)°$ and $\alpha_2 = (-109 \pm 3)°$ with respect to the closed packed Cu rows and $(-72 \pm 3)°/(-120 \pm 3)°$ for 0.10 ML (not shown). The error bars were determined from the χ^2 variation; using only one angle to describe the rotation of both molecules in the unit cell leads to an increase in χ^2 from 0.003 to 0.024 and is clearly outside the error bar. These angles are the basis for the models shown in Figure 10.** Because of the mirror symmetry of Cu{110} with respect to the $[\bar{1}10]$ direction the angles describing the orientation of L-serine must have opposite signs.

Summary and Discussion

In summary, our experimental LEED and STM data show that L/D serine overlayers on Cu{110} form well-ordered superstructures with $(-1 \mp 2; 4\ 0)$ periodicity after annealing. In the STM images dimers can be resolved, each occupying one unit cell of the superstructure, which are tilted by $\beta = \mp 73°$ (L/D) with respect to the $[\bar{1}10]$ direction of the close packed rows of Cu atoms. The XPS data indicate that both molecules in the dimer are in a deprotonated anionic state (OHCH$_2$CNH$_2$COO) and form bonds with the surface Cu atoms through the two oxygen atoms of the carboxylate group and the nitrogen atom of the amino group. The β-OH side group is intact and is available for hydrogen bonds with adjacent molecules. The azimuthal angles of the carboxylate groups of the two inequivalent serine molecules in the ordered L/D dimer struc-

tures are determined from NEXAFS as $\alpha_1 = \pm 79°$ and $\alpha_2 = \pm 109°$ with respect to $[\bar{1}10]$ (see

Figure 10(a)). For low coverage these angles are different by about $10°$ such that the carboxylate

groups are tilted further away from the close packed rows of Cu atoms, which is still within the

range of values determined for other amino acids, such as glycine and alanine, on Cu{110}.[22,31,44]

Figure 10(a) shows four different dimer structures for D-serine, which are compatible with the

experimental data for the ordered layer at saturation coverage. The differences between the models

are whether angle α_1 is associated with the molecule on the left (I and II) or on the right (III and

IV) and whether the intra-dimer bond involves a carboxylate group (I and III) or just the amino

and β-OH groups (II and IV). For clarity, hydrogen atoms are omitted in Figure 10(a) but the H-

bonds are indicated by dashed lines. Significant stabilization due to hydrogen-bonding has been

proposed for de-protonated glycine and alanine on Cu{110} on the basis of model calculations and

spectroscopic evidence from NEXAFS.[20,25,26,31,32,53] In these cases H-bonds are formed between

the COO oxygen atoms and NH_2. They stabilize the adsorbate by 0.2-0.4 eV per molecule[20,32]

and, thus, favor islands over isolated molecules at low coverage. Nyberg et al. assigned a peak at

536 eV in the O-NEXAFS of glycinate on Cu{110} to H-bonding between the carboxylate group

and NH_2.[20] We observe the same peak in the $-90°$ NEXAFS spectrum of the saturated layer. The

angular dependence indicates that the corresponding H-bond is close to the $[\bar{1}10]$ direction.

The carboxylate groups are deprotonated, therefore no hydrogen bonds can be formed between

them. This implies that only the dimers of models I and III could form hydrogen bonds with neigh-

boring dimers and thus aggregate into ordered islands at low coverages, as is observed in LEED

and STM. We can therefore eliminate models II and IV. Of the remaining two models I appears

more likely for geometric reasons since suitable $OH \cdots OCO \cdots NH_2$ hydrogen bond lengths can

be achieved without major distortion of the molecules. Figure 10(b) shows a comparison of this

model with the STM data for the ordered L and D-serine layers. Intra-dimer hydrogen-bonds are

formed between β-OH and NH_2 groups and the two oxygen atoms of the same carboxylate group,

whereas the hydrogen bonds between the dimers involve the COO group and either the β-OH or

the NH_2 group of adjacent molecules, which leads to the staggered arrangement observed by STM.

For L-serine on Cu{100} a different intra-dimer bonding, through two $H_2N\cdots OCO$ linkages, has been proposed in order to explain the peanut shape found in STM experiments by Iwai et al.[29] In this model only amino and carboxylate groups are involved in the intra-dimer bond whereas the links between dimers involve hydrogen bonds between the β-OH, amino and carboxylate groups. This type of dimers is not compatible with the molecular orientation found in our STM and NEX-AFS experiments. The local arrangements of neighboring serine molecules on Cu{110} and {100} are therefore very different, which indicates that there is no hierarchy of inter-molecular bonds. Inter-dimer and intra-dimer bonds are equally important in stabilizing the dimer structures and the local inter-molecular bond geometry adjusts to the substrate lattice, which provides the primary covalent adsorption bonds. In the gas phase serine forms stable homochiral octamers, which involve H-bonding between all side groups.[41,42,54] The sub-units of the octamer structure consist of dimers linked by H-bonding between carboxylic acid groups. The links between the dimers are hydrogen-bonds between NH_2 and β-OH moieties, similar to the bonds in the bulk crystal structure of serine.[48]

Dimer formation has not been observed for glycine, alanine or proline on Cu{110} or Cu{100},[3,10,12,13,17,21,22,] also the pairing observed for alanine and glycine on Cu{531} cannot be considered as true dimer formation as it only involves one hydrogen bond rather than two per pair.[6,37,40] Cysteine on Au{110}, however, forms homochiral dimers through two $OH\cdots O$ bonds involving the intact carboxylic acid groups.[19] Since there are several ways of forming dimers of amino acids it is not possible to pinpoint a particular side group that is necessary for their occurrence.

For low coverage (0.07-0.11 ML) both enantiomers form ordered islands at room temperature. The periodicity, is the same as for the saturated layer after annealing. NEXAFS shows small differences in the molecular orientation of around 10°, which is probably due to the larger relative contribution of molecules at the island boundaries. The shape of the serine islands at low coverage is highly anisotropic and indicates a preferred growth direction vectors $\vec{w}_1$ and $\vec{w}_2$, respectively, in Figure 2, Figure 6(III), or Figure 10(b). The same anisotropy has been observed by LEED and STM on two different crystals and appears to be largely independent of the orientation of substrate step

16

edges. The STM images of Figure 6(IIIa,b) were obtained from a Cu{110} surface with a slight miscut such that the L-serine islands have their prevalent growth direction nearly perpendicular to the step edges, whereas the growth direction for D-serine lies primarily along the steps. Suitably oriented and spaced steps could, thus, be used to limit the island size of one enantiomer vs the other. Our data set is too small to determine whether this anisotropy in the growth behavior is a kinetic effect or due to the energetics of hydrogen bonds near the island boundaries. The fact that the first desorption peak in the TPD spectra of enantiopure layers at low coverage is 28 K lower than for saturation coverage (cf Figure 4) indicates a significant global stabilization through the hydrogen-bond network in large islands. This is equivalent to a significant reduction in adsorption energy associated with island boundaries and it is likely that this reduction is different for boundaries perpendicular and parallel to the growth direction.

It is remarkable that almost no isolated monomers or dimers were observed in the STM images. Deposition of intermediate to high coverages at room temperature, however, led to a significant amount of monomers within hydrogen-bonded aggregates (cf Figure 5(b,c) and Figure 6(Ia)). After annealing, all monomers were converted into dimers, which shows that their formation has a relatively high activation barrier once the molecule is involved in a hydrogen-bonded network. On the other hand, the network plays an important role in stabilizing the dimers. They, therefore, have to be seen as sub-units of an extended hydrogen-boned structure rather than as stand-alone units.

The differences between L and D-serine in dimer orientation and dimer stacking with respect to the underlying achiral substrate lead to spontaneous chiral resolution of the racemic mixture and into small enantiopure domains. By comparison with the enantiopure layers the chirality of dimers in the racemic layers can be identified on the basis of their orientation with respect to the underlying substrate. From the images in Figure 7 it becomes clear that the enantiopure domains formed from L and D-serine dimers have the same structure as those observed for the enantiopure molecules, even the anisotropy in the island shape is the same. We did not find any evidence in the STM images for new structures unique to racemic serine, which strongly indicates that dimer formation occurs only between equal enantiomers. The enantiopure domains in the racemic layer

17

are, in general, smaller than in the enantiopure layers and the separation is not perfect, even after annealing to 370 K. Heterochiral stacking faults within the domains disrupt the formation of large islands, which is also apparent from the relatively broad spots in the LEED pattern (Figure 3). Also, the lower temperature of the first desorption peak in TPD for the saturated racemic layer as compared to the enantiopure layers is an indication of smaller islands with fewer hydrogen bonds contributing to the stabilization of the molecules.

As pointed out above, suitably nanostrutures surfaces with steps along the growth direction of one enantiomer and narrow terraces would only allow molecules of this enantiomer to grow large islands whereas the others would be limited by the terrace width. Together with the fact that molecules are more stable in large islands than in small islands this could provide a pathway for separating enantiomers on a macroscopic scale. A similar chiral separation process would also be possible for Cu{100} where serine also forms globally chiral superstructures.[29]

Conclusion

Chemisorbed serine on Cu{110} is in its de-protonated anionic form when deposited at room temperature at low coverage or at high coverage after annealing. The L/D enantiomers aggregate in well-ordered islands with $(-1 \mp 2; 4\ 0)$ periodicity consisting of one serine dimer per surface unit cell. By using a combination of STM, LEED, and NEXAFS we show that the chirality of the adsorption system is expressed at three levels: the orientation of homochiral dimers, the superstructure lattice formed by the dimers, and the growth anisotropy of small islands. In racemic mixtures chiral resolution into small ordered enantiopure islands appears to be driven by the formation of homochiral dimer subunits and the directionality of inter-dimer hydrogen bonds. These islands show the same enantiospecific elongated shapes as in low-coverage enantiopure layers.

Acknowledgements

References

(1) Hazen, R. M.; Filley, T. R.; Goodfried, G. A. *Prog. Natl. Acad. Sci. USA* **2001**, *98*, 5487 – 5490.

(2) Hazen, R. M.; Sholl, D. S. *Nature Mat.* **2003**, *2*, 367.

(3) Barlow, S. M.; Raval, R. *Surf. Sci. Rep.* **2003**, *50*, 201.

(4) Baddeley, C. *Top. Catal.* **2003**, *25*, 17.

(5) Ma, Z.; Zaera, F. *Surf. Sci. Rep.* **2006**, *61*, 229–281.

(6) Held, G.; Gladys, M. J. *Top. Catal.* **2008**, *48*, 128.

(7) Baddeley, C. J.; Held, G. *Chiral Molecules on Surfaces*, 1st ed.; Comprehensive Nanoscience and Technology; Elsevier: Amsterdam, 2010.

(8) Baiker, A. *J. Mol. Catal. A* **1997**, *115*, 473.

(9) Baiker, A. *J. Mol. Catal. A* **2000**, *163*, 205.

(10) Williams, J.; Haq, S.; Raval, R. *Surf. Sci.* **1996**, *368*, 303.

(11) Löfgren, P.; Krozer, A.; Lausmaa, J.; Kasemo, B. *Surf. Sci.* **1997**, *370*, 277.

(12) Barlow, S. M.; Kitching, K. J.; Haq, S.; Richardson, N. V. *Surf. Sci.* **1998**, *401*, 322.

(13) Booth, N. A.; Woodruff, D. P.; Schaff, O.; Gießel, T.; Lindsay, R.; Baumgärtel, P.; Bradshaw, A. M. *Surf. Sci.* **1998**, *397*, 258.

(14) Zhao, X.; Gai, Z.; Zhao, R. G.; Yang, W. S.; Sakura, T. *Surf. Sci.* **1999**, *424*, L347.

(15) Zhao, X.; Zhao, R. G.; Yang, W. S. *Surf. Sci.* **1999**, *442*, L995.

(16) Zhao, X. *J. Am. Chem. Soc.* **2000**, *122*, 12584–12585.

(17) Chen, Q.; Frankel, D. J.; Richardson, N. V. *PhysChemComm, 1999, 9* **1999**, *1999*, 9.

(18) Chen, Q.; Frankel, D. J.; Richardson, N. V. *Surf. Sci.* **2002**, *497*, 37.

(19) Kühnle, A.; Linderoth, T. R.; Hammer, B.; Besenbacher, F. *Nature* **2002**, *415*, 891.

(20) Nyberg, M.; Odelius, M.; Nilsson, A.; Petterson, L. G. M. *J. Chem. Phys.* **2003**, *119*, 12577.

(21) Barlow, S. M.; Louafi, S.; Le Roux, D.; Williams, J.; Muryn, C.; Haq, S.; Raval, R. *Surf. Sci.* **2005**, *590*, 243.

(22) Sayago, D. I.; Polcik, M.; Nisbet, G.; Lamont, C. L. A.; Woodruff, D. P. *Surf. Sci.* **2005**, *590*, 76.

(23) Gonella, G.; Terreni, S.; Cvetko, D.; Cossaro, A.; Mattera, L.; Cavalleri, O.; Rolandi, R.; Morgante, A.; Floreano, L.; Canepa, M. *J. Phys. Chem. B* **2005**, *109*, 18003–18009.

(24) Rankin, R. B.; Sholl, D. S. *Surf. Sci.* **2004**, *548*, 301.

(25) Rankin, R. B.; Sholl, D. S. *Surf. Sci. Lett.* **2005**, *574*, L1.

(26) Rankin, R. B.; Sholl, D. S. *J. Phys. Chem. B* **2005**, *109*, 16764 – 16773.

(27) Iwai, H.; Tobisawa, M.; Emori, A.; Egawa, C. *Surf. Sci.* **2005**, *574*, 214–218.

(28) Ghiringhelli, L. M.; Schravendijk, P.; Delle Site, L. *Phys. Rev. B* **2006**, *74*, 035437.

(29) Iwai, H.; Emori, A.; Egawa, C. *Surf. Sci.* **2006**, *600*, 1670–1673.

(30) Iwai, H.; Egawa, C. *Langmuir* **2010**, *26*, 2294 – 2300.

(31) Jones, G.; Jones, L. B.; Thibault–Starzyk, F.; Seddon, E. A.; Raval, R.; Jenkins, S. J.; Held, G. *Surf. Sci.* **2006**, *600*, 1924.

(32) Jones, G.; Jenkins, S. J.; King, D. A. *Surf. Sci.* **2006**, *600*, L224–L228.

(33) Blankenburg, S.; Schmidt, W. G. *Phys. Rev. B* **2006**, *74*, 155419.

(34) Blankenburg, S.; Schmidt, W. G. *Nanotechnology* **2007**, *18*, 424030.

(35) Gao, F.; Li, Z.; Wanga, Y.; Burkholder, L.; Tysoe, W. T. *J. Phys. Chem. C* **2007**, *111*, 9981 – 9991.

(36) Gao, F.; Li, Z.; Wanga, Y.; Burkholder, L.; Tysoe, W. T. *Surf. Sci.* **2007**, *601*, 3276 – 3288.

(37) Gladys, M. J.; Stevens, A. V.; Scott, N. R.; Jones, G.; Batchelor, D.; Held, G. *J. Phys. Chem. C* **2007**, *111*, 8331–8336.

(38) Schiffrin, A.; Riemann, A.; Auwärter, W.; Pennec, Y.; Weber-Bargioni, A.; Cvetko, D.; Cossaro, A.; Morgante, A.; Barth, J. V. *PNAS* **2007**, *104*, 5279–5284.

(39) Forster, M.; Dyer, M. S.; Persson, M.; Raval, R. *J. Am. Chem. Soc.* **2009**, *131*, 10173–10181.

(40) Eralp, T.; Zheleva, Z. V.; Shavorskiy, A.; Dhanak, V. R.; Held, G. *Langmuir* **2010**, *26*, 10918–10923.

(41) Cooks, R. G.; Zhang, D.; Koch, K. J.; Gozzo, F. C.; Eberlin, M. N. *Anal. Chem.* **2001**, *73*, 3646–3655.

(42) Nanita, S. C.; Cooks, R. G. *Angewandte Chemie -International Edition* **2006**, *45*, 554–569.

(43) Ammon, C.; Bayer, A.; Steinrück, H. P.; Held, G. *Chem. Phys. Lett* **2003**, *377*, 163–169.

(44) Hasselström, J.; Karis, O.; Weinelt, M.; Wassdahl, N.; Nilsson, A.; Nyberg, M.; Petterson, L. G. M.; Samant, M. G.; Stöhr, J. *Surf. Sci.* **1998**, *407*, 221.

(45) Feulner, P.; Menzel, D. *J. Vac. Sci. Tech.* **1980**, *17*, 662.

(46) Lægsgaard, E.; Besenbacher, F.; Mortensen, K.; Stensgaard, *J. Microscopy* **1988**, *152*, 663–669.

(47) Feyer, V.; Plekan, O.; Skala, T.; Chab, V.; Matolin, V.; Prince, K. C. *J. Phys. Chem. B* **2008**, *112*, 13655–13660.

(48) Kistenmacher, T. J.; Rand, G. A.; Marsh, R. E. *Acta Cryst. B* **1975**, *30*, 2573.

(49) Petoral, R. M.; Uvdal, K. *Journal of Electron Spectroscopy and Related Phenomena* **2003**, *128*, 159–164.

(50) Weinhold, M.; Soubatch, S.; Temirov, R.; Rohlfing, M.; Jastorff, B.; Tautz, F. S.; Doose, C. *J. Phys. Chem. B* **2006**, *110*, 23756–23769.

(51) Thomsen, L.; Wharmby, M.; Riley, D. P.; Held, G.; Gladys, M. J. *Surf. Sci.* **2009**, *603*, 1253 – 1261.

(52) Stöhr, J. *NEXAFS spectroscopy*, 2nd ed.; Springer Series in Surface Sciences; Springer: Berlin, 1996.

(53) Rankin, R. B.; Sholl, D. S. *J. Chem. Phys.* **2006**, *124*, 074703.

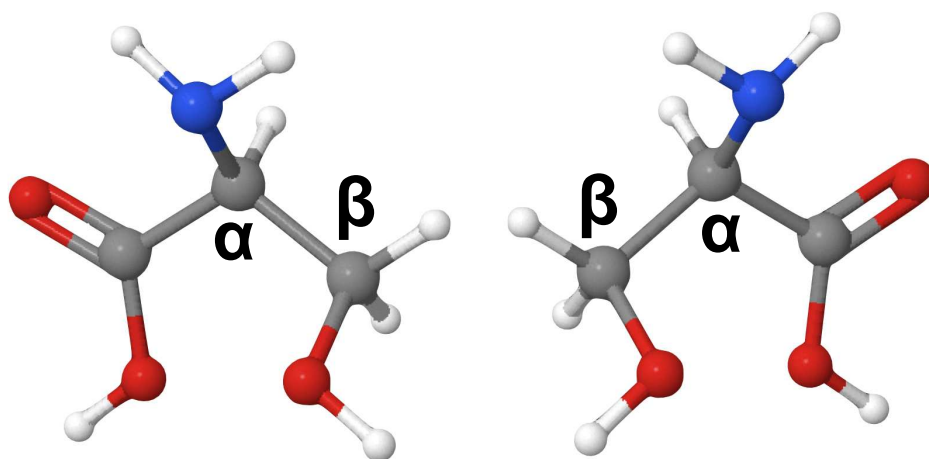(54) Takats, Z.; Nanita, S. C.; Schlosser, G.; Vekey, K.; Cooks, R. G. J. *Anal. Chem.* **2003**, *75*, 6147–6154.

Figure 1: Molecular structure models of L and D-serine in the gas phase (left and right, respectively)
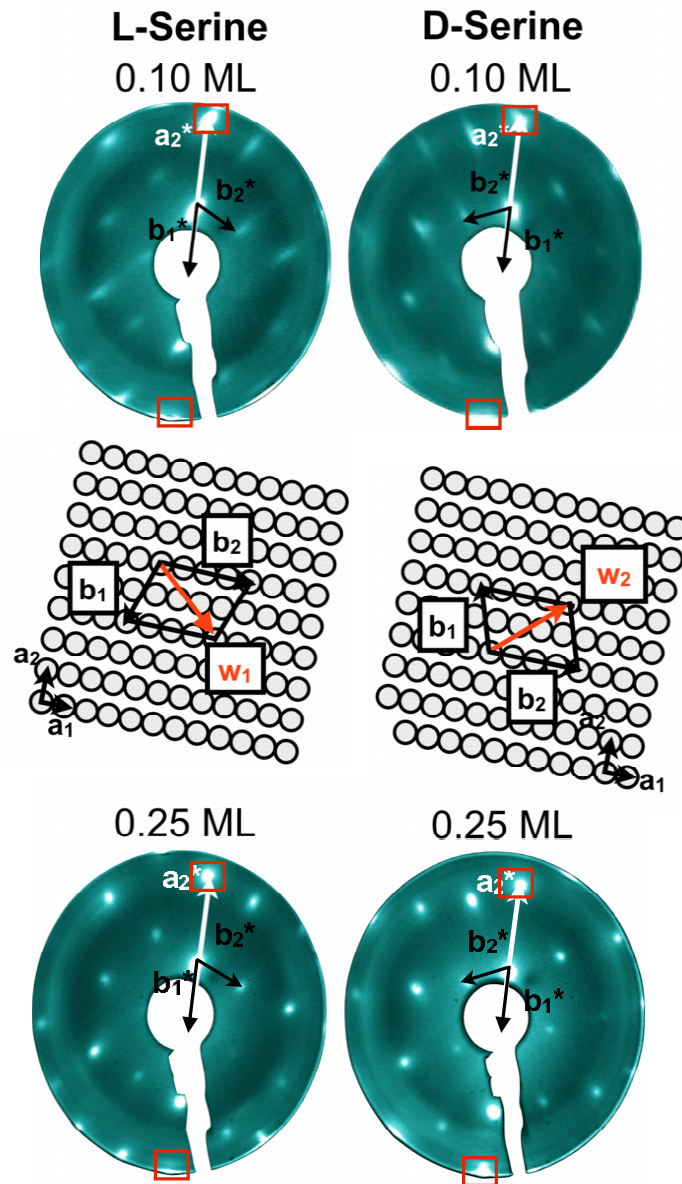
Figure 2: Top: LEED images for 0.1 ML L-serine and D-serine on Cu{110} deposited room temperature. Bottom: LEED images of saturated chemisorbed layers (0.25 ML) of L-serine and D-serine annealed to 420 K. The reciprocal overlayer unit cell vectors, $\vec{b}_1^*$ and $\vec{b}_2^*$, and the substrate reciprocal unit cell vector $\vec{a}_2^*$ are indicated in the LEED images (Electron energy = 28 eV in all images, the integer-order spots are indicated by squares). Middle: Real space model of the Cu{110} surface with the unit cell vectors $\vec{b}_1$, $\vec{b}_2$ (black) and the broadening direction of domains for low coverage $\vec{w}_1$ and $\vec{w}_2$ (red).
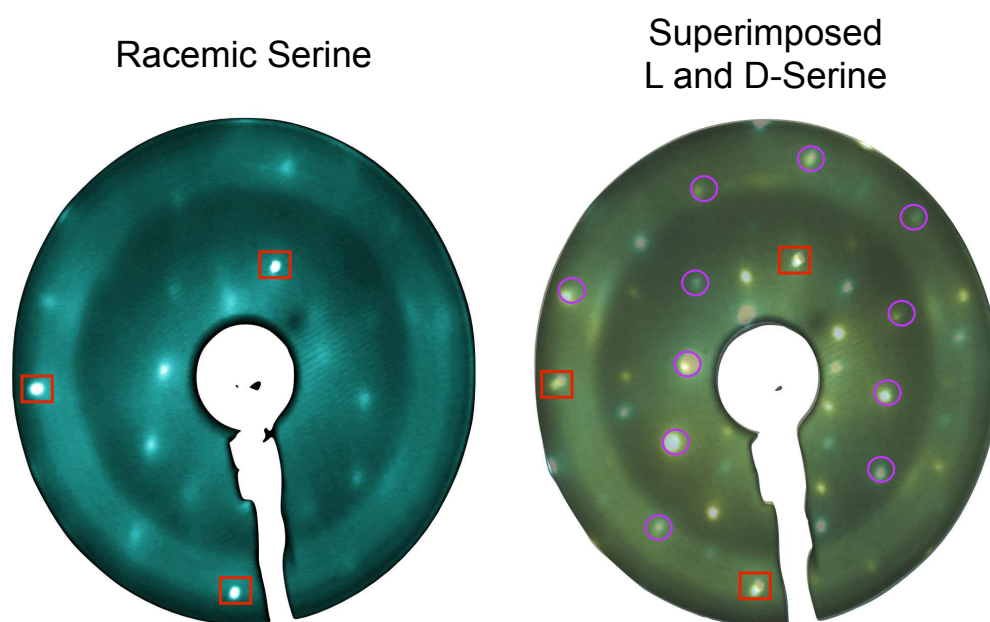
Figure 3: Left: LEED image of a saturated chemisorbed layer of racemic serine on Cu{110}, annealed to 420 K. Right: Superposition of LEED images of saturated enantiopure L- and D-serine layers; overlapping spots are marked by circles. (Electron energy = 57 eV in both images, the interger-order spots are highlighted by squares)
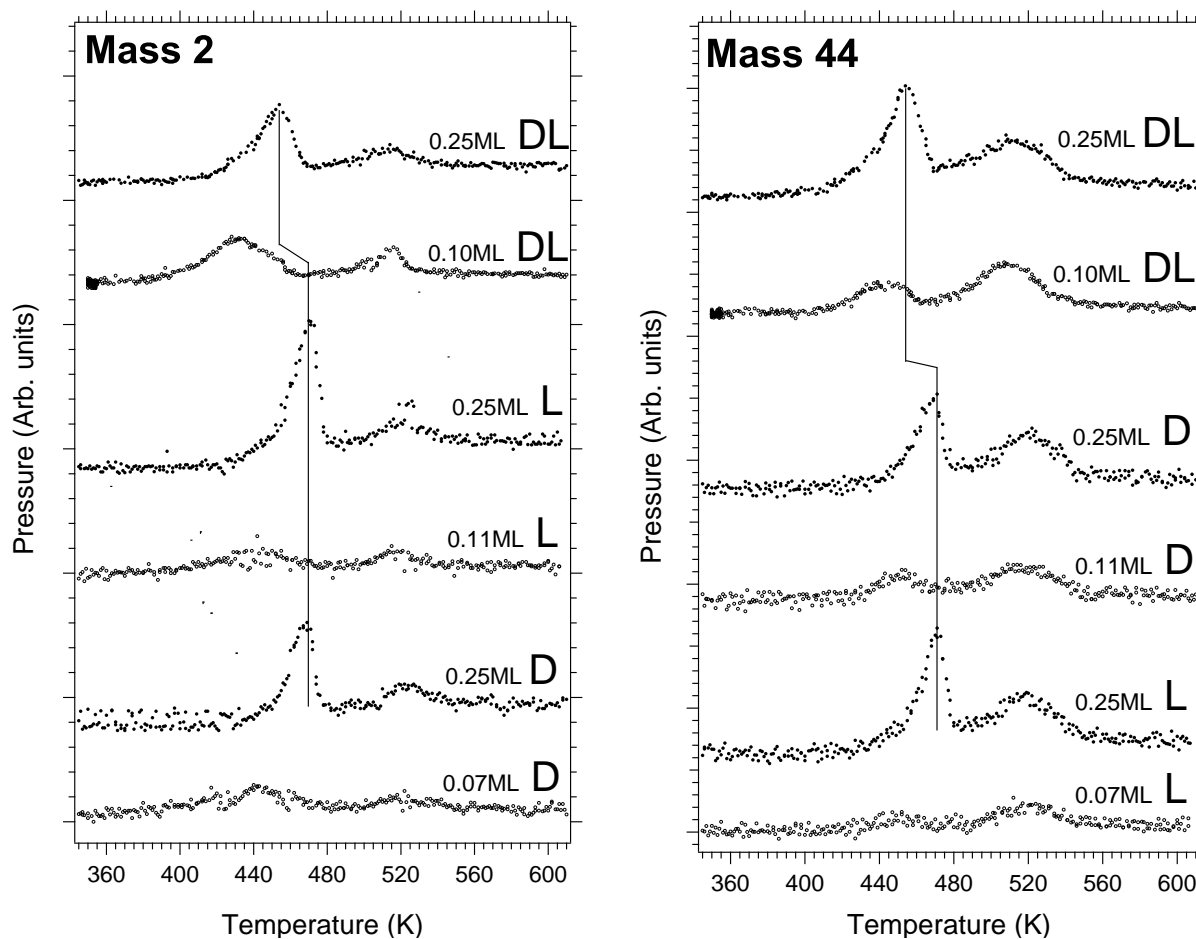
Figure 4: TPD spectra of saturated and lower coverage (≈ 0.1 ML) chemisorbed layers of L, D and racemic (LD) serine. Left: H_2 partial pressure vs temperature; right: CO_2 partial pressure vs temperature.
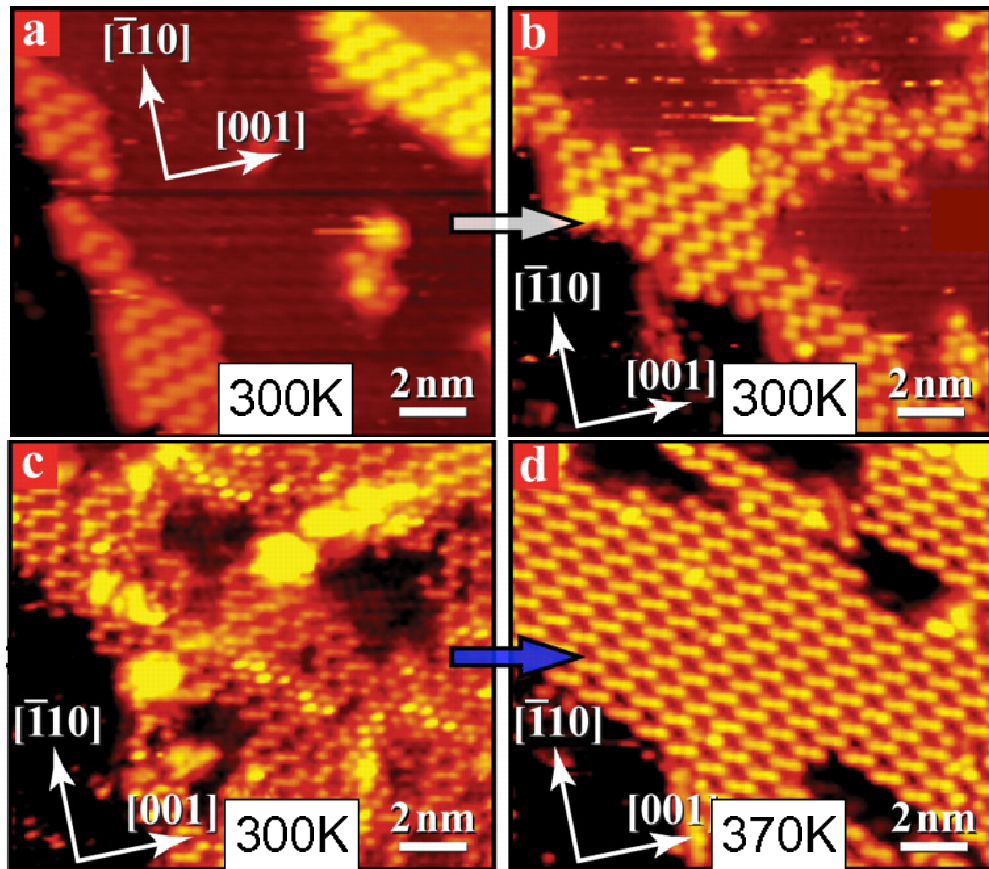
Figure 5: STM images of adsorption structures formed by D-serine on Cu{110}. (a) Low coverage (0.03 ML) prepared at room temperature; (b) intermediate coverage (0.08 ML) at room temperature; (c) high coverage (0.19 ML) at room temperature; (d) same coverage annealed to 370 K. (I_{tip} = -0.33/-0.52/-0.65/-0.42 nA, V_{tip} = -1317/-1250/-999/-1095 mV in a/b/c/d)
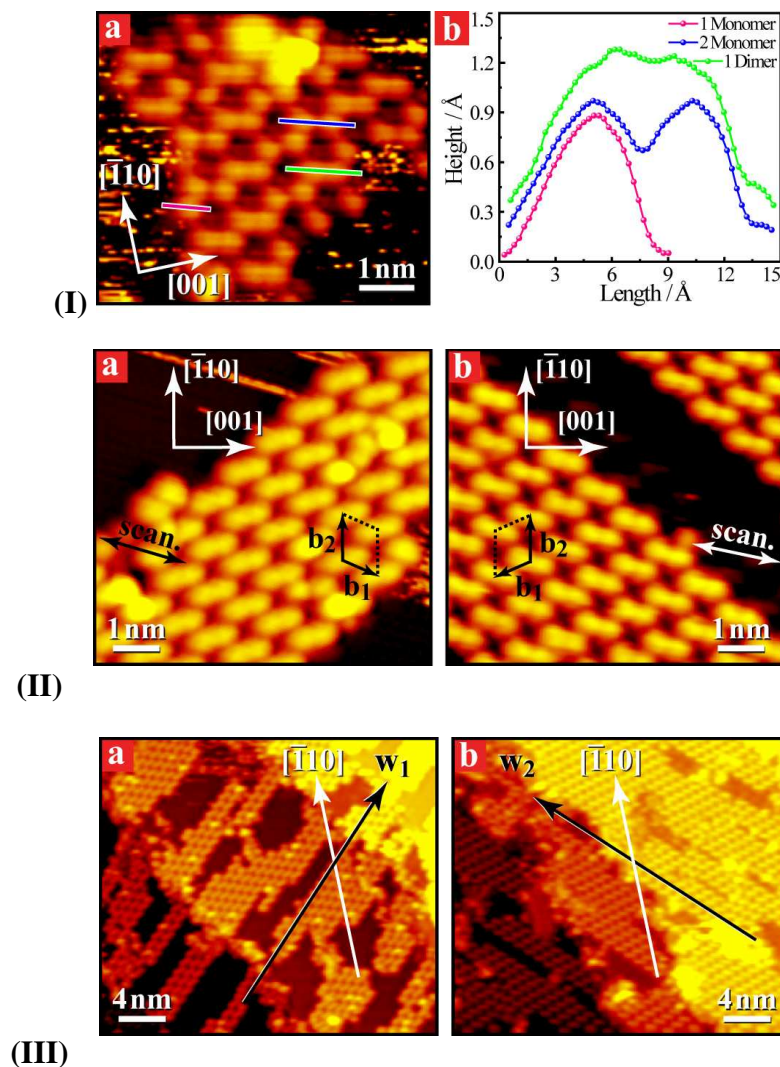
(I)

(II)

(III)

Figure 6: I: (a) STM image of molecular island formed by a layer of 0.08 ML D-serine on Cu{110} at room temperature, showing both monomer and dimer features (I_{tip} = -0.65 nA, V_{tip} = -1250 mV); (b) height profiles taken along the lines indicated in the STM image for a serine monomer (pink line), two monomers in contact (purple line) and a dimer (green line). II: Ordered islands formed by (a) L- and (b) D-serine dimers on Cu{110} after annealing to 370 K. The figure panels show cut-outs from STM images which have been rotated to bring the $[\bar{1}10]$ direction vertical, making the mirror-image relation between the structures formed by the two enantiomers apparent. The fast scan direction for the respective images is indicated by double arrows. Unit cells for both domains are shown by the b_1 and b_2 vectors. (I_{tip} = -0.48/-0.37 nA, V_{tip} = -1250/-1096 mV in a/b) III: Larger-scale STM images showing the island growth behavior for (a) L- and (b) D-serine on the Cu{110} surface. The preferential island growth directions ($\vec{w}_1$ and $\vec{w}_2$) are indicated for both enantiomers. The $[\bar{1}10]$ crystallographic direction of the substrate is shown. (I_{tip} = -0.48/-0.39 nA, V_{tip} = -1250/-1277 mV in a/b)
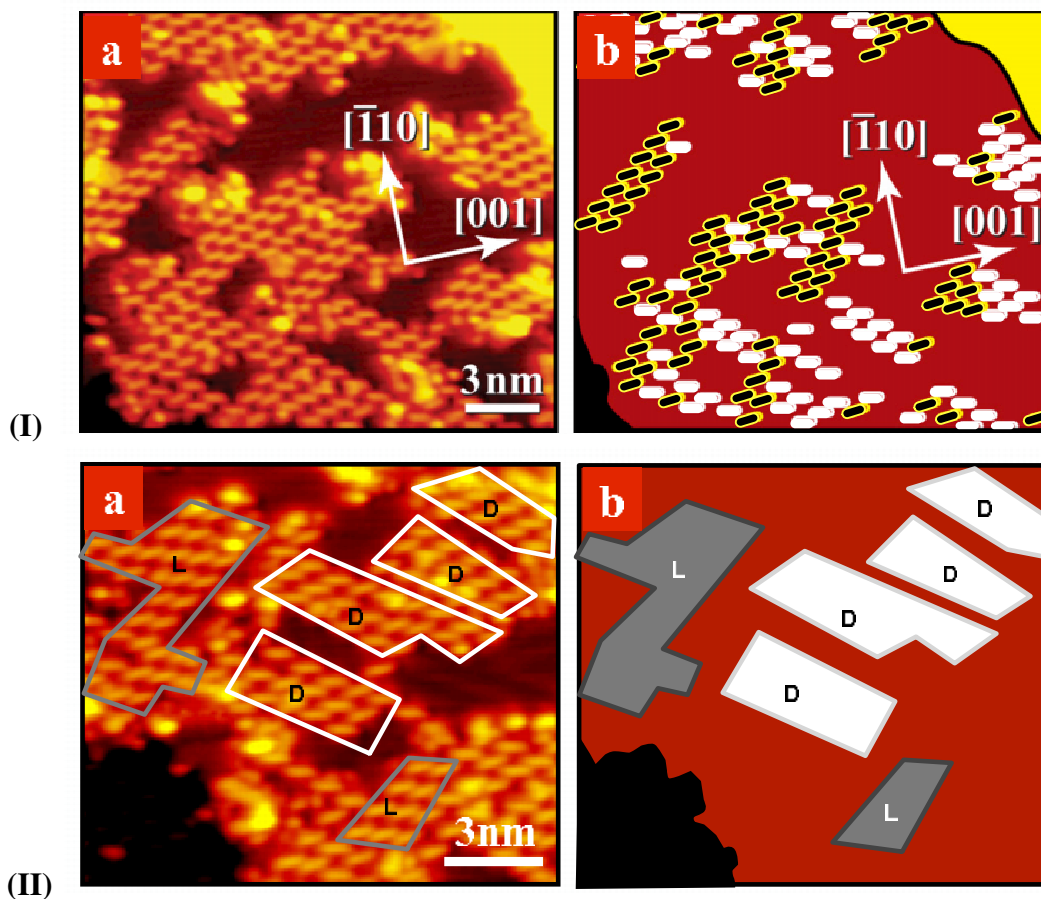
Figure 7: High coverage locally-ordered layer (0.17 ML) of racemic serine on Cu{110}. I: (a) STM image; (b) corresponding sketch of the molecular pattern where L- and D-serine dimers are indicated by yellow (dark) and white (light) ovals, respectively, showing segregation into small enantiopure domains. II: (a) STM image of another part of the same layer; (b) and schematic drawing of the domain distribution. (I_{tip} = -0.39 nA, V_{tip} = -1250 mV)
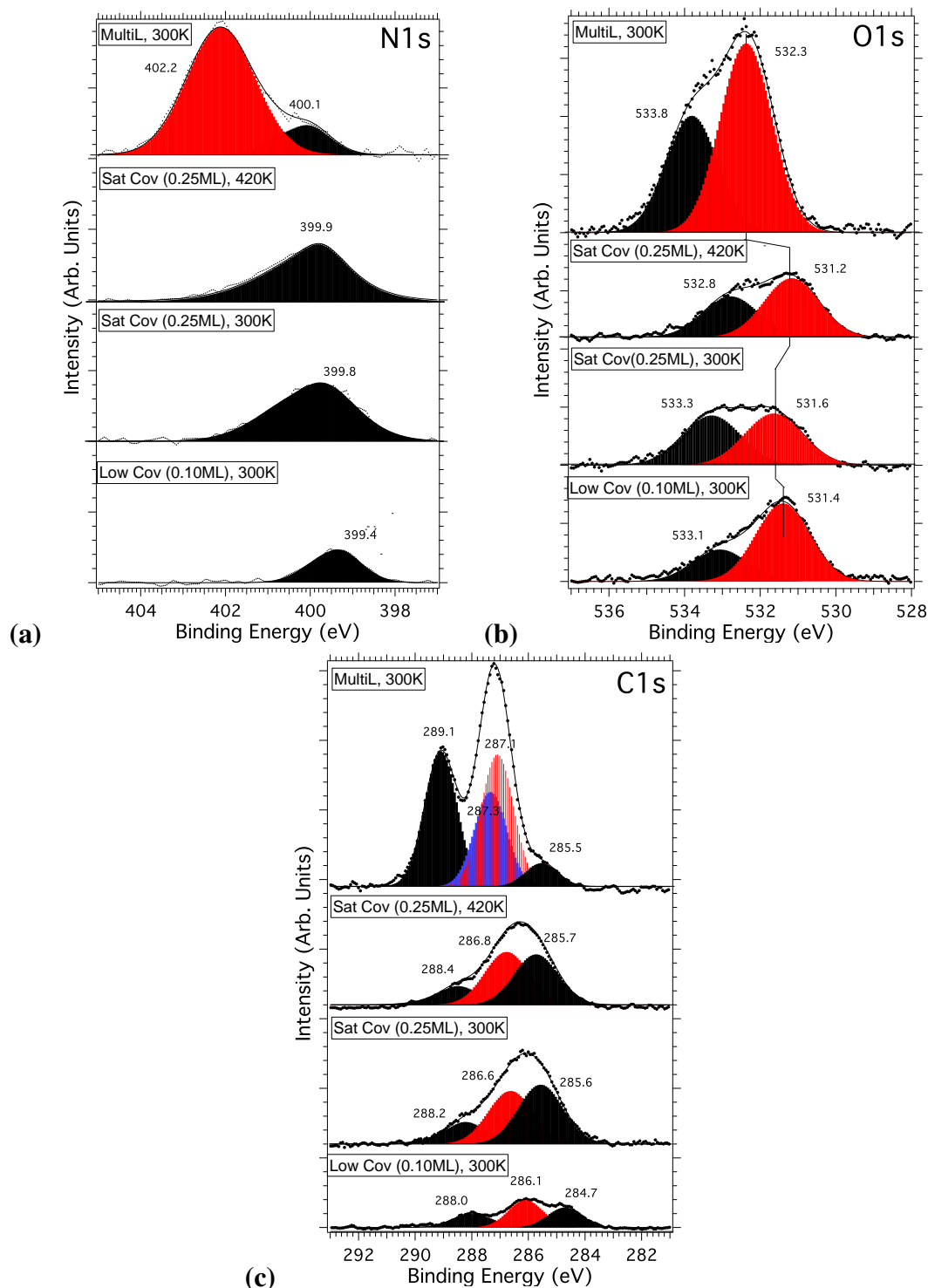
Figure 8: (a) N 1s XP Spectra of D-serine adsorbed on Cu{110} (Photon Energy = 510 eV); (b) O 1s XP Spectra of D-serine adsorbed on Cu{110} (Photon Energy = 635 eV); (c) C 1s XP Spectra of D-serine adsorbed on Cu{110} (Photon Energy = 400 eV).
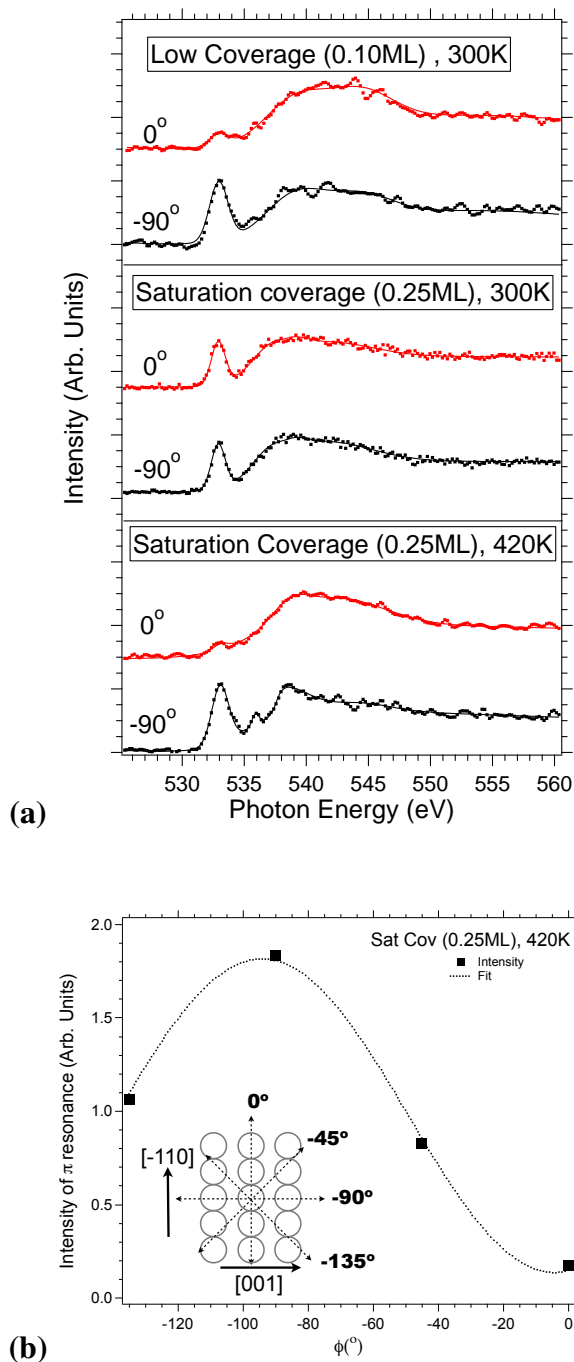
(a)

(b)

Figure 9: (a) O-NEXAFS spectra of D-serine on Cu{110} for two orthogonal orientations of the polarization vector ($0°$ and $-90°$). Top: 0.1 ML at room temperature; middle: saturated chemisorbed layer at room temperature; bottom: saturated chemisorbed layer annealed to 420 K at polarization angles; (b) Intensity of the π-resonance of the saturated chemisorbed layer (annealed to 420 K) vs polarization angle (squares) and fit of the data with the sum of $\cos^2$ functions describing the angular dependence of two molecules (see text for details). The inset shows the alignment of the angular scale with the crystallographic directions.
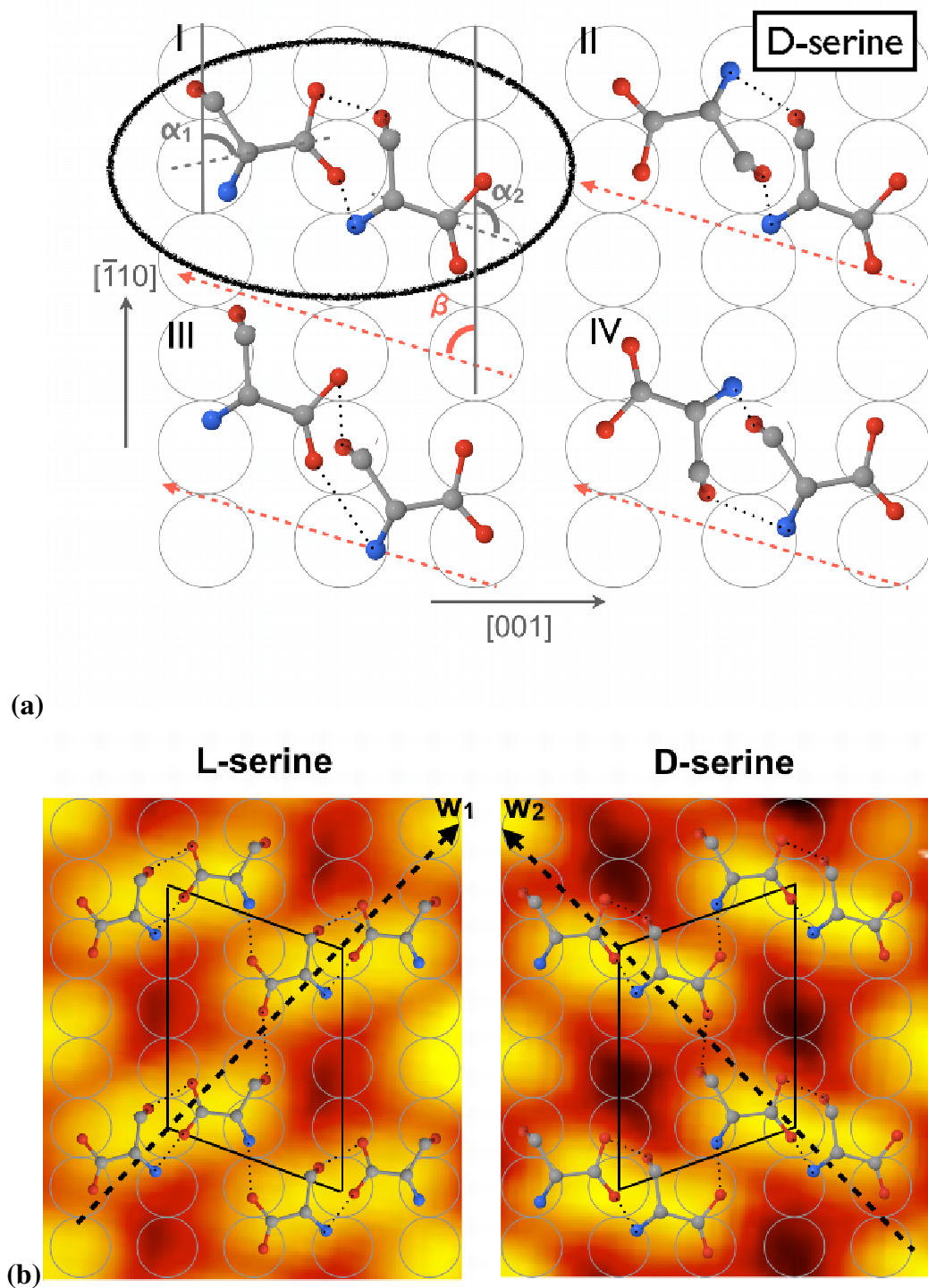
(a)

(b)

Figure 10: (a) Models for D-serine dimers on Cu{110}, which are compatible with the triangular footprint of O,O,N bonding and the angles $\alpha_{1,2}$ determined by NEXAFS; the angle β indicates the dimer orientation determined by STM. Hydrogen atoms are omitted for clarity but hydrogen-bonds are indicated by dashed lines; model (I) is the preferred model (see text for details). (b) Overlay of the proposed model (I) onto the experimental STM images of the ordered L and D serine layers. H-bonds and unit cells are indicated; $\vec{w}_1$ and $\vec{w}_2$ represent the island growth directions.